



Ian J. Taylor
Lecturer, Department of
Mechanical Engineering,
University of Strathclyde,
Glasgow, UK



Andrew C. Robertson
Research Student,
Department of Mechanical
Engineering, University of
Strathclyde, Glasgow, UK



Stephen K. Wilson
Head of Department,
Department of Mathematics,
University of Strathclyde,
Glasgow, UK



Brian R. Duffy
Senior Lecturer, Department
of Mathematics, University of
Strathclyde, Glasgow, UK



Julie M. Sullivan
Research Student,
Department of Mathematics,
University of Strathclyde,
Glasgow, UK

New developments in rain–wind-induced vibrations of cables

I. J. Taylor PhD, CEng, MIMechE, A. C. Robertson MEng, S. K. Wilson MA, MSc, DPhil, FIMA,
B. R. Duffy MA, MSc, PhD and J. M. Sullivan BSc

On wet and windy days, the inclined cables of cable-stayed bridges can experience large amplitude, potentially damaging oscillations known as rain–wind-induced vibration (RWIV). RWIV is believed to be the result of a complicated non-linear interaction between rivulets of rain water that run down the cables and the wind loading on the cables from the unsteady aerodynamics; however, despite a considerable international research effort, the underlying physical mechanism that governs this oscillation is still not satisfactorily understood. An international workshop on RWIV was held in April 2008, hosted at the University of Strathclyde. The main outcomes of this workshop are summarised in the paper. A numerical method to investigate aspects of the RWIV phenomenon has recently been developed by the authors, which couples an unsteady aerodynamic solver to a thin-film model based on lubrication theory for the flow of the rain water to ascertain the motion of the rivulets owing to the unsteady aerodynamic field. This novel numerical technique, which is still in the relatively early stages of development, has already provided useful information on the coupling between the external aerodynamic flow and the rivulet, and a summary of some of the key results to date is presented.

NOTATION

B	solid body in unsteady aerodynamic solver
C_D	coefficient of drag
$\overline{C_D}$	mean (time-averaged) coefficient of drag
$\overline{C_F}^*$	normalised mean (time-averaged) coefficient of friction
C_L	coefficient of lift
$\overline{C_L}$	mean (time-averaged) coefficient of lift
$\overline{C_P}$	mean (time-averaged) coefficient of pressure
F	flow field in unsteady aerodynamic solver
g	acceleration owing to gravity
H, h	thickness of water film on surface of cylinder (normal to surface)
i, j, k	unit orthogonal vectors
n, n	unit vector and distance normal to body surface
P, p	pressure distribution
Q	azimuthal volume flux of fluid in the film
R	radius of cylinder

Re	Reynolds number = UD/ν where D is the cable diameter
r	position vector
r, θ, z	polar coordinates with the z axis along the axis of the cylinder and θ measure from upstream stagnation point
S	surface of body in unsteady aerodynamic solver
s, s	unit vector and distance tangential to body surface
T	shear distribution
t	time
U, U	velocity magnitude and vector
u, v	horizontal and vertical velocities
x, y	horizontal and vertical directions
α	cable inclination angle
β	cable yaw angle (angle of cable to wind direction)
γ	surface tension of water
$\varepsilon (= H/R)$	ratio of thickness of film to cylinder radius
ζ	damping ratio
θ	angle around circumference of cylinder from stagnation point
κ	mean curvature of the free surface of the film
μ	dynamic viscosity of fluid
ν	kinematic viscosity of fluid
ρ	density of fluid
Ψ	vector potential and stream function
Ω	rotational velocity of solid body
ω, ω	vorticity (vector and magnitude)

1. INTRODUCTION

On wet and windy days, the inclined cables of cable-stayed bridges can experience large amplitude oscillations known as rain–wind-induced vibration (RWIV). Since the phenomenon was first reported by Hikami in 1988 (Hikami and Shiraishi, 1988), RWIV has been the focus of a considerable amount of research activity in the international wind- and bridge-engineering communities. Despite this research effort, a full understanding of the aeroelastic phenomenon has yet to be obtained owing to the complexity of the interaction between the rivulets of rain water running down the inclined cable, the unsteady aerodynamic flow field and the structural dynamics of the cable.

Data from full-scale investigations and wind tunnel experiments undertaken since the original observation of Hikami and Shiraishi (1988) have provided a sizeable

knowledge base concerning the conditions under which RWIV most commonly occurs. Notable examples of bridges on which RWIV has been investigated are the Erasmus Bridge, Rotterdam, the Netherlands (Geurts *et al.*, 1998), the Fred Hartman Bridge, Baytown, Texas (Zuo *et al.*, 2008), and the Dongting Lake Bridge, Hunan Province, China (Ni *et al.*, 2007).

In summary, these data suggest that RWIV tends to occur only over a restricted range of wind velocities, typically between 5 and 15 m/s (Table 1), under ‘moderate’ rain conditions for cables that descend in the direction of the wind ($0^\circ < \beta < 180^\circ$) in terms of the angles defined in Figure 1. (A consistent definition of ‘moderate’ rain cannot be obtained from the published research.) Cable inclination angles, α , are typically between 20° and 50° , and yaw angles, β , are typically between 20° and 50° . The cables themselves normally have diameters in the range 100 to 250 mm, and have low structural damping ($\zeta \leq 0.5\%$), while the response is generally in the frequency range 0.6 to 3 Hz and normally occurs in the cable-pylon plane (Figure 1). Through such characteristics RWIV can be identified as a distinct aeroelastic phenomenon, with particular features that distinguish it from other aeroelastic instabilities such as galloping or vortex-induced vibration.

One of the key aspects of the RWIV instability is the presence and location of the rivulets of rain water on the surface of the cable. In experiments, it has been observed that the thin film of rain water present on the cable normally accumulates to form two rivulets near the separation points of the external aerodynamic field around a dry cable (Bosdogianni and Olivari, 1996). Other studies have concentrated on specific aspects of the location and dynamics of the rivulet motion, to identify the effect of the rivulets on the external aerodynamic field and vice versa. The latter investigations can be broadly separated into two distinct classes: those where the rivulet is replaced by a fixed, static, rigid protuberance – that is, an ‘artificial rivulet’ (Bosdogianni and Olivari, 1996; Matsumoto *et al.*, 1995) and those where a film of water is sprayed onto the surface of the cable and the rivulets are allowed to form ‘naturally’ (Cosentino *et al.*, 2003; Flamand, 1995; Gu and Du, 2005; Verwiebe and Ruscheweyh, 1998; Wang *et al.*, 2005). Both classes indicate that the presence of the rivulet on the upper surface is largely responsible for the vibration (Matsumoto *et al.*, 1995), while the latter class also indicates that when free to do so, the rivulets oscillate circumferentially at the same frequency as that with which the cable vibrates. Differentiating between the effect of circumferential oscillation and rivulet position in the ‘artificial rivulet’ investigations has, however,

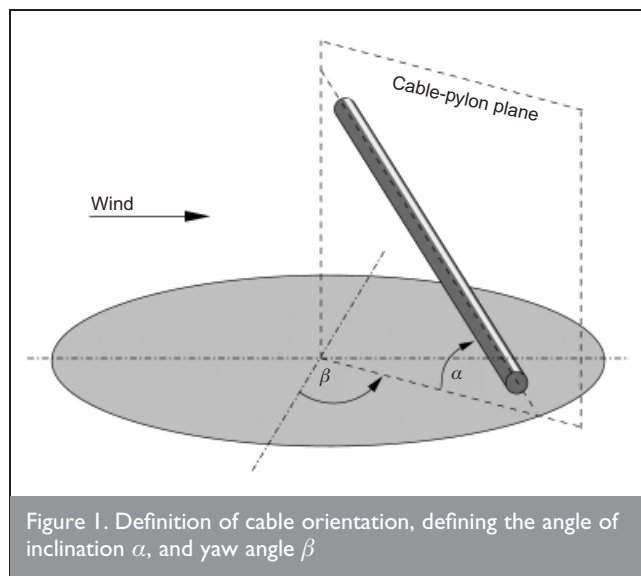


Figure 1. Definition of cable orientation, defining the angle of inclination α , and yaw angle β

proved more difficult and led to discrepancies in the literature. In particular Verwiebe and Ruscheweyh (1998) determined that the circumferential oscillation of the rivulet is a primary cause of RWIV, whereas Bosdogianni and Olivari (1996) suggest that it is rivulet location and not its profile or circumferential oscillation which initiates the response.

Several analytical models have also been developed to investigate RWIV, most of which are loosely based on the work of Yamaguchi (1990), wherein the RWIV mechanism is modelled as a two-dimensional (2D), multiple mass, multiple degree of freedom (DOF), spring mass damper system, with aerodynamic forces determined using a quasi-steady approximation. These analytical models share several common features, but also present distinct differences determined by the exact nature of the specific aspect under investigation, two such examples being a 2DOF model with a circumferentially movable rigid attachment representing the ‘artificial rivulet’ (Gu and Huang, 2008), and a 4DOF three mass model to investigate the differences between laminar and turbulent flow on the cable–rivulet system response (Peil and Dreyer, 2007). Seidel and Dinkler (2006) investigated stable locations for the rivulets; however in this instance the focus was on determining the differences between sub-critical and critical flow fields. The rivulets were considered as moveable disturbances, and the aerodynamic coefficients were determined using a theoretical approach based on Prandtl’s tripwire phenomenon.

Bridge/wind tunnel	Wind-speed range: m/s
Meiko-Nishi West Bridge (Hikami and Shiraishi, 1988)	7–14
Erasmus Bridge (Geurts <i>et al.</i> , 1998)	14
Fred Hartman Bridge (Zuo <i>et al.</i> , 2008)	5–15
Dongting Lake Bridge (Ni <i>et al.</i> , 2007)	6–14
Three bridges (Matsumoto <i>et al.</i> , 1995)	6–17
Wind tunnel (Flamand, 1995)	7–12
Wind tunnel (Gu <i>et al.</i> , 2002)	12–17
Wind tunnel (Cosentino <i>et al.</i> , 2003)	7–12

Table 1. Mean wind speed ranges reported for RWIV from full-scale observations and wind tunnel investigations

Despite all of this analytical work, however, computational models for RWIV are scarce owing to the complexity of the problem and the need to couple models for the thin film of rain water, the unsteady aerodynamic field, and the structural dynamics of the cable. To date, the majority of the numerical investigations of RWIV have focused on fixed rigid artificial rivulets, with 2D and three-dimensional (3D) large eddy simulations (LESs) examining the effect that static rivulets have on the overall flow field (Li and Gu, 2006, Liu *et al.*, 2007). Lemaitre *et al.* (2007) presented a different approach using lubrication theory and the time-averaged flow-field over a circular cylinder to ascertain the evolution of the rain water rivulets.

Research in the Departments of Mechanical Engineering and Mathematics at the University of Strathclyde has focused on developing a numerical model to investigate aspects of RWIV. The approach adopted is to couple a modified pre-existing unsteady aerodynamic solver for the external aerodynamic flow field with a solver based on a thin-film model for the evolution and deformation of the water rivulets. Results from the individual models will be presented herein along with preliminary results from fully coupled simulations of the problem.

2. INTERNATIONAL WORKSHOP ON RAIN-WIND-INDUCED VIBRATION

An international workshop on RWIV was hosted by the University of Strathclyde on 30 March to 1 April 2008. The workshop was hosted by the authors of the current paper at Ross Priory, a conference facility owned by the University of Strathclyde on the banks of Loch Lomond. The aim was to bring a number of the key international experts in the field of RWIV together to present and discuss their latest research findings on the phenomenon. The workshop format provided much more time for focused and open discussion than is usually possible in a normal conference environment, allowing the current ideas and uncertainties on the underlying physics to be established and future research directions to be identified. Funding for the meeting was provided by the University of Strathclyde Research Enhancement Fund. The delegates who attended the meeting are shown in Figure 2.

2.1. Summary of the research presented

During the workshop, delegates presented recent and ongoing research on RWIV, in a more informal style than at conventional conferences. A brief summary of the content of these presentations is given below, followed by the main research themes that arose from the discussions.

The University of Strathclyde researchers highlighted the recent numerical developments in both the Department of Mechanical Engineering and Department of Mathematics, the results of which will be summarised later in this paper. In addition Professor Stephen Wilson and Ms Julie Sullivan described some of the recent work in the Department of Mathematics on thin rivulets and ridges of fluid subject to prescribed longitudinal and/or transverse shear-stress effects at their free surface (Sullivan, 2009; Sullivan *et al.*, 2008).

Professor Matsumoto and Dr Yagi summarised the extensive research that has been conducted at Kyoto University.



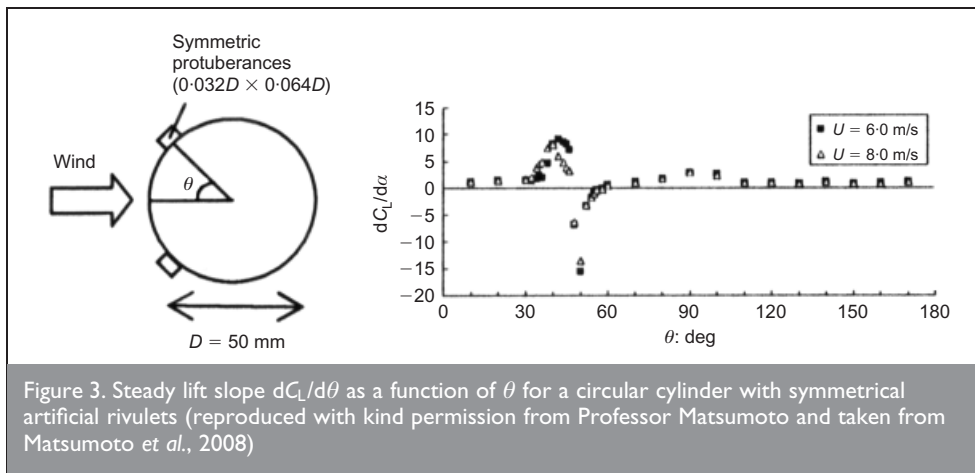
Figure 2. The participants in the International Workshop on Rain-Wind Engineering, held at Ross Priory, University of Strathclyde, 30 March–1 April 2008. From left to right : Professor Stephen Wilson, Dr Brian Duffy, Dr Xiaoqing Du, Dr John Macdonald, Dr Olivier Flamand, Prof. Masaru Matsumoto, Dr Pascal Hemon, Dr Delong Zuo, Dr Ian Taylor, Ms Julie Sullivan, Dr Tomomi Yagi, Mr Andrew Robertson

Particular themes included the role of the axial vortex on inclined cables (Matsumoto *et al.*, 2001), the sensitivity of inclined cables to dry-state galloping (Matsumoto *et al.*, 2007a), and the importance of Karman vortex suppression during the cable response associated with the negative lift slope when rivulets are present close to the separation points ((Matsumoto *et al.*, 2001; Matsumoto *et al.*, 2007a). Figure 3 illustrates experimental results for artificial rivulets that exhibit the strong negative lift slope at about 50°.

Dr Flamand presented results from a series of wind tunnel tests which demonstrated that the surface characteristics of the cable play a strong role in the RWIV instability, notably for 'dirty' cables (Flamand, 1995) and RWIV mitigation devices such as helical wires. Recent results (Cosentino *et al.*, 2003) indicate that the water present on the cable forms a 'base carpet' of constant height, on which an 'oscillating wave' (the rivulet) slides. The frequency of this movement is the same as that of the cable motion, with the rivulet shape strongly influenced by inertia effects.

Dr Du gave a wide-ranging summary of the research at Tongji University, China, under the leadership of Professor Ming Gu. In particular, he presented high-resolution pressure measurements illustrating the effect of artificial rivulets on the flow (Gu, 2007; Gu and Du, 2005; Gu and Huang, 2008), and results from theoretical models highlighting that when rivulets are present at certain circumferential locations the lift coefficient drops significantly and a galloping-type instability is observed (Gu, 2007).

Dr Hemon presented recent experimental and numerical investigations focusing on the rivulet dynamics. Recent numerical computations have used lubrication theory to predict rivulet growth and evolution under a constant pressure loading, with two distinct rivulets being found to form at approximately the separation points of a dry circular cylinder under all the loadings examined (Lemaitre *et al.*, 2007).



full-scale observations, it is often problematic to classify or identify occurrences as either one type of instability or the other. Reanalysis of previous data has demonstrated that the two phenomena are not as distinct as previously thought. The general consensus was that the two phenomena are related, or are even potentially the same, and that the presence of rain water rivulets enhances or acts as a catalyst for the

Dr Zuo provided details of numerous full-scale investigations from the Fred Hartman Bridge, Houston, Texas, USA, reflecting on how reanalysis of existing data possibly changes the assessment of this instability (Zuo *et al.*, 2008). Although comparisons of RWIV with vortex-induced vibration (VIV) illustrate similarities between the two phenomena, suggesting that RWIV may be attributable to a type of VIV excitation, the effect of the rivulets remains unclear.

oscillation, perhaps ‘widening the window’ for galloping. However, these ideas have not been conclusively demonstrated, and there are several unanswered questions as to the role of the rivulets on the overall flow field.

Dr Macdonald summarised recent research on analytical modelling of dry-inclined galloping using a quasi-steady approach (Macdonald and Larose, 2008a, 2008b). A number of conjectures on the similarities between RWIV and dry-inclined galloping were considered, notably the effect of the critical Reynolds number and associated drag crisis on both instabilities.

Considering the two instabilities as similar or related phenomena, however, may not be straightforward, as there have been instances of RWIV at fairly low speed and at sub-critical Reynolds numbers, which is not consistent with the general characteristics of dry-inclined galloping. Macdonald also confirmed that instances of ‘dry’ vibrations at low wind speed have been reported, probably at sub-critical Reynolds numbers, where the oscillations are in a transverse or across-wind direction, which are not explainable by the quasi-steady theory. Recent numerical research from Yeo and Jones (2008) investigates the flow past a dry inclined cable at sub-critical Reynolds numbers. The results illustrate how swirling eddies are generated alternately from both sides of the cylinder but also move along the cylinder thus delaying the vortex shedding. This flow feature causes unsteady forces that vary both spatially and temporally in the spanwise direction, thus generating a low frequency loading on the cable. These results will provide a useful comparison for future investigations on the effect of rivulets on the 3D flow field around an inclined cable and their role in the generation or modification of the unsteady aerodynamic loading.

2.2. Discussion: key research themes and future research directions

A main theme of the discussion was how RWIV can be categorised. The instability is distinct in many ways, thus meriting its own classification as a unique aeroelastic phenomenon. However, as outlined above, recent research has suggested that the phenomenon has characteristics related to a number of other instabilities which make it difficult to classify.

Reynolds number effects, particularly in the critical region, appear to be important to the mechanisms of both dry-inclined galloping and RWIV. Subsequently the ‘single-bubble’ phenomenon may play an important role, as identified by Cosentino *et al.* (2003). (The ‘single-bubble’ region appears for flow close to the critical region, where one shear layer undergoes transition to a turbulent state, resulting in it separating later than the other shear layer, leading to asymmetric flow.) This is a possible aspect of the RWIV mechanism that has not been fully investigated to date, with the role of the rivulets in enhancing or causing the single-bubble regime still not clear.

- (a) Comparisons between full-scale observations and dry-inclined galloping results indicate noticeable similarities between these two instabilities, particularly the effect of the critical Reynolds number regime.
- (b) Rivulets located close to the separation points can suppress the Karman vortex, increasing the susceptibility of the cable to a galloping-type instability.
- (c) The presence of a low-frequency axial vortex behind the inclined cable can cause a vortex-induced instability at high reduced velocity. The presence of rain water rivulets in certain locations on the cable surface can enhance this instability and the magnitude of the response (Matsumoto *et al.*, 2001, 2003).
- (d) Similarities between classical VIV and RWIV have been identified, although RWIV occurs at higher reduced velocity and with higher amplitude than VIV.

Rivulets located close to the separation point have a strong effect on the overall response, and rivulets at certain locations on the surface can cause large negative lift slopes, thus increasing the susceptibility to galloping (Matsumoto *et al.*, 2007a, 2008). Examples were given by both Flamand and Hemon of instances where a dry cable did not oscillate, but

The similarities between dry-inclined galloping and RWIV were a particular focus of the discussions. From experiments and

under the same flow conditions the introduction of water onto the surface of the cable initiated oscillations. This indicates that the presence of the water is a key factor in the mechanism, although the role of the surface characteristics of the cable is not fully understood.

All of the delegates felt that the development of a numerical tool to investigate RWIV was important and could provide valuable data that have the potential to give important insights into the underlying physical mechanism of RWIV. However, the complexity of the problem has to date limited the development of a full numerical model. It was noted that any proposed model should incorporate numerical solutions of the Navier–Stokes equations for both the aerodynamic field and the water rivulets along with equations for the cable dynamics, and provide accurate unsteady pressure results.

The main conclusions from the international workshop can therefore be summarised as follows.

- (a) Despite considerable international research activity over the last two decades, the RWIV phenomenon is still not well understood.
- (b) RWIV is related to, but distinct from, dry-inclined galloping.
- (c) The presence of rivulets can act to increase the likelihood of a galloping-type oscillation.
- (d) Vibrations often occur in flow regimes in which Karman vortex shedding is suppressed.
- (e) RWIV often occurs in the critical Reynolds number range. However, the precise role of the drag crisis and the ‘single-bubble regime’ has not yet been fully established.
- (f) There is still a large degree of uncertainty as to the exact role played by the size, shape and location of the rivulets and the effect of surface characteristics.
- (g) Improved numerical methods are required to aid understanding of RWIV, to provide information not presently obtainable from experiments and to help clarify several aspects of the phenomenon.

Furthermore, all of the delegates agreed that a similar workshop should be arranged in the future, in order to continue to stimulate ideas, communication and collaboration, and to further enhance understanding of RWIV.

3. NUMERICAL MODELLING OF RWIV

A numerical model for RWIV has been developed at the University of Strathclyde. The numerical approach used is to couple a thin-film model based on lubrication theory to an unsteady aerodynamic solver, the latter being a modified version of the DIVEX code developed at the Universities of Strathclyde and Glasgow, which has previously proven successful with unsteady, incompressible, highly separated flows such as those under investigation (Taylor and Vezza, 1999, 2001, 2002). The thin-film model is based on an analytical model developed by the Department of Mathematics, which has a long track record of internationally recognised theoretical research into a wide variety of both steady and unsteady viscous thin-film flows, notably rivulet flows (Holland *et al.*, 2001; Wilson and Duffy, 2005; Sullivan *et al.*, 2008). The collaboration and complementary skills of the two departments provides a unique team of researchers with the

necessary capabilities to develop a numerical model for RWIV. A summary of some of the key results to date from this collaborative research is presented along with an indication of possible future research directions.

3.1. The discrete vortex method

The governing equations used in the numerical model are the vorticity-stream function form of the continuity equation and the Navier–Stokes equations for 2D incompressible viscous flow

$$1 \quad \nabla^2 \Psi = -\omega$$

$$2 \quad \frac{\partial \omega}{\partial t} + (\mathbf{U} \cdot \nabla) \omega = \nu \nabla^2 \omega$$

where the vorticity ω is defined as the curl of the velocity (Equation 3) and Ψ is a vector potential (Equation 4)

$$3 \quad \omega = \nabla \times \mathbf{U} \quad \text{with} \quad \omega = \omega k$$

$$4 \quad \mathbf{U} = \nabla \times \Psi, \quad \nabla \Psi = 0 \quad \text{with} \quad \Psi = \Psi k$$

The far field boundary conditions (Equation 5), and no-slip and no-penetration conditions (Equation 6) apply at infinity and the surface of the body, respectively

$$5 \quad \mathbf{U} = \mathbf{U}_\infty \quad \text{or} \quad \nabla \Psi = \nabla \Psi_\infty \quad \text{on} \quad S_\infty$$

$$6 \quad \mathbf{U} = \mathbf{U}_i \quad \text{or} \quad \nabla \Psi = \nabla \Psi_i \quad \text{on} \quad S_i$$

where subscripts ∞ and i respectively denote the far field and the i th body ($i = 1, 2, \dots, m$, with m being the number of solid bodies). Proper definition of the problem allows only one of the normal and tangential boundary conditions at the body surface to be explicitly applied. In the current formulation, this is the normal component no-penetration condition. However, the tangential no-slip condition is implicitly satisfied due to the representation of the internal kinematics of each solid body. The velocity at a point \mathbf{r} on the surface of or within body i can be described by

$$7 \quad \mathbf{U}_i = \mathbf{U}_{ic} + \boldsymbol{\Omega}_i \times (\mathbf{r}_p - \mathbf{r}_{ic})$$

where \mathbf{r}_{ic} is a fixed reference point on the body. This may be represented in stream-function form as

$$8 \quad \nabla^2 \Psi_i = -2\Omega_i \quad \text{in} \quad B_i$$

Application of Green’s theorem to Equations 1 and 8, together with boundary conditions Equations 5 and 6, allows a relationship between velocity and vorticity to be obtained. The velocity field can then be calculated using the Biot–Savart law,

which expresses it in terms of the vorticity field. For a point p in the fluid, the velocity is given by

$$U_p = U_\infty + \frac{1}{2\pi} \int_F \omega \frac{k \times (r_p - r)}{\|r_p - r\|^2} dF + \int_{B_i} 2\Omega_i \frac{k \times (r_p - r)}{\|r_p - r\|^2} dB_i$$

The pressure distribution on the body surface can then be evaluated by integrating the pressure gradient along the body contour, which is given by

$$\frac{1}{\rho} \frac{\partial P}{\partial s} = -s \frac{DU_c}{Dt} - \mathbf{n} \cdot (\mathbf{r} - \mathbf{r}_c) \frac{D\Omega}{Dt} + s \cdot (\mathbf{r} - \mathbf{r}_c) \Omega^2 + \nu \frac{\partial \omega}{\partial n}$$

The resulting pressure distribution can then be integrated around the body surface to calculate the aerodynamic forces on the body and the moment about the body reference point, \mathbf{r}_{ic} , at a particular computational time step. Further statistical measures such as time-averaged mean coefficients may then be determined. For a more detailed presentation of the details as they relate to the present numerical implementation the reader is referred to Taylor and Vezza (1999).

3.2. Mathematical modelling of the rivulet dynamics

Two-dimensional unsteady flow of a thin film of incompressible viscous fluid with uniform dynamic viscosity μ and density ρ on the outer surface of a stationary horizontal circular cylinder of radius R is considered. The free surface of this film is subject to a prescribed normal stress ('pressure'), $\mathbf{P} = \mathbf{P}(\theta, t)$, and prescribed tangential stress ('shear'), $\mathbf{T} = \mathbf{T}(\theta, t)$, exerted by the external aerodynamic field (Figure 4). The evolution equation for the water thickness on the cylinder surface, $h(\theta, t)$, is given by

$$h_t + \left[-\frac{1}{3\mu R} \left(\rho g \cos \theta - \frac{\mathbf{y}}{R^3} (h + h_{\theta\theta})_\theta + \frac{\mathbf{P}_\theta}{R} \right) h^3 + \frac{\mathbf{T}h^2}{2\mu R} \right]_\theta = 0,$$

the full derivation of which is given in the Appendix. Equation 11 is consistent with the corresponding equation given by Lemaitre *et al.* (2007) in the case of flow on a static cylinder. This equation is to be solved subject to an initial condition of the form $h(\theta, 0) = h_0(\theta)$, where $h_0(\theta)$ is the initial thickness of the film. For definiteness in the present work an initially uniform film $h_0 = \text{constant}$ has been chosen, and the film was allowed to evolve according to Equation 11 to see if 2D 'rivulets' develop.

4. RESULTS OF THE NUMERICAL INVESTIGATION

4.1. Investigation of artificial rivulets

A numerical investigation to ascertain the effect of the circumferential location of artificial rivulets on the overall flow field was undertaken. As Robertson and Taylor (2007) describe in more detail, the artificial rivulet used is a trapezoidal profile

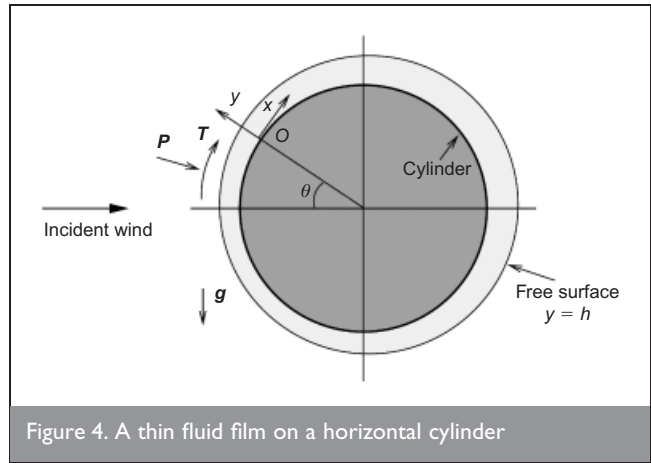


Figure 4. A thin fluid film on a horizontal cylinder

and is a similar size and shape to those used in recent wind tunnel studies (Figure 5(a)). In all cases, a sub-critical Reynolds number, $Re = 2 \times 10^4$ (based on the cable diameter), was used and is consistent with the lower wind speed range for RWIV.

Two combinations of rivulet geometry, referred to as single and multiple symmetric rivulet (Figure 5(b)), are presented herein. A multiple antisymmetric configuration is also presented by Robertson and Taylor (2007). These particular arrangements were chosen to best represent possible rivulet configurations governed by a single angular parameter, θ .

4.1.1. Single rivulet. The upper rivulet is thought to play the greatest role in RWIV. As such, the primary study examined

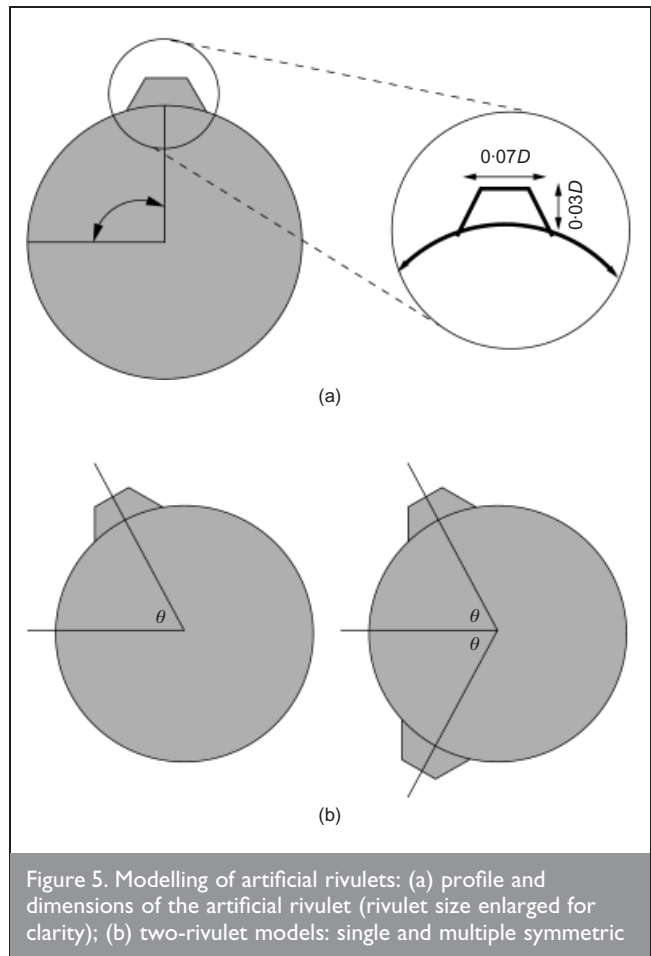


Figure 5. Modelling of artificial rivulets: (a) profile and dimensions of the artificial rivulet (rivulet size enlarged for clarity); (b) two-rivulet models: single and multiple symmetric

the variation of aerodynamic force coefficients on the cylinder with angle of the attached rivulet from incident flow, θ . The variation of predicted time-averaged mean aerodynamic forces with rivulet location is shown in Figure 6, where the lift shows good agreement with results from experimental data (Matsumoto *et al.*, 2007b).

The presence of the rivulet on the cable surface leads to four distinct flow regimes which can be clearly identified in the aerodynamic force results. At angles $\theta < 45^\circ$ the attached rivulet has little effect on either of the mean aerodynamic coefficients (lift \bar{C}_L and drag \bar{C}_D) in comparison to the dry cylinder case, as the rivulet is located too close to the front of the cylinder for it to have a significant effect on the separation of the shear layers and wake formation. The rivulet does cause a local separation of the shear layer, although at these low angles the flow almost immediately reattaches to the cylinder, with full separation occurring only at the same location as a dry cylinder. Hence the overall mean loadings are not strongly affected, as is also demonstrated by the experimental results, where the lift is determined to be zero until approximately 35° . The experiments (Matsumoto *et al.*, 2007b) used a slightly higher Reynolds number of 2.6×10^4 , which may give some explanation for the increase in lift occurring at a slightly lower angle owing to the effect of Re on the boundary-layer formation.

At $\theta \cong 45^\circ$ a sudden change in flow regime occurs, with a rapid increase in time-averaged mean lift coefficient and a corresponding but much smaller decrease in time-averaged mean drag coefficient. This occurs because the rivulet is now sufficiently far from the stagnation point that it causes the boundary layer to trip, thus influencing the location of the separation point on the upper side of the cylinder. This transition to turbulent flow on the upper side causes the flow to detach at a greater angle from incidence than the laminar flow on the lower (non-rivulet) side, which results in an asymmetric flow field generating a positive lift force, towards the side of the rivulet.

At angles above $\theta \cong 60^\circ$ the tripped flow on the upper surface

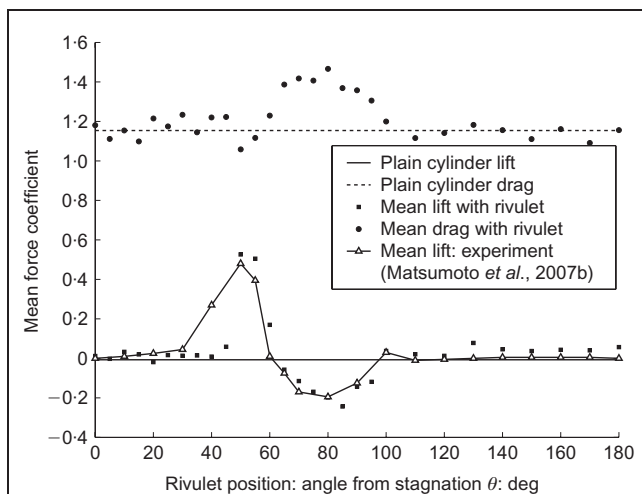


Figure 6. Variation of \bar{C}_D and \bar{C}_L with rivulet angle θ for the single artificial rivulet case, compared with experimental data from Matsumoto *et al.* (2007b)

detaches from the cylinder at the rivulet location, and this probably occurs earlier than on the lower surface. The resulting asymmetric flow with negative lift (towards the opposite side from the rivulet) and the increase in cross-flow wake size are caused by the detachment of the flow, which also results in an increase in the drag.

When the angle is greater than $\theta \cong 100^\circ$, the rivulet is located sufficiently far past the separation point to ensure that it is in the region of the cylinder surface that is immersed in the wake and thus has a negligible impact on the aerodynamic properties of the body itself.

Crucially in the second of these regimes, $50^\circ < \theta < 60^\circ$, unlike at any other angular position, Karman vortex shedding is suppressed and no clear Strouhal frequency can be detected. The negative lift curve slope in this region suggests that this could lead to a potential galloping instability, and at these angles the Den Hartog criterion $(dC_L/d\theta) + C_D < 0$ was found to be valid.

4.1.2. Multiple symmetric rivulets. In this case the rivulets are located symmetrically at equal angles clockwise and anticlockwise from the incident flow. The predicted variation of \bar{C}_L with θ is shown in Figure 7. These results demonstrate features that are consistent with phenomena discussed in the single rivulet case. Notably the symmetry of the problem gives zero mean lift over almost the entire range of rivulet angle, and hence in this case no galloping instability could occur. (Symmetry means that $(dC_L/d\theta) \approx 0$ at all angles, so the Den Hartog criterion is not satisfied.) The exception occurs when $\theta \cong 50^\circ$, where experiments (Matsumoto *et al.*, 2008) have shown that the flow field is very sensitive to small changes in the rivulet position. This sensitivity is still being investigated in the present numerical study and will be fully reported in future. Distinct similarities to the single rivulet case are also apparent in the \bar{C}_D profile, one example being the increase in mean drag coefficient in the range $60^\circ < \theta < 100^\circ$ owing to the detachment of the flow, resulting in a wider wake.

4.1.3. Oscillating rivulet. Simulations were undertaken with the rivulet oscillating sinusoidally with constant amplitude

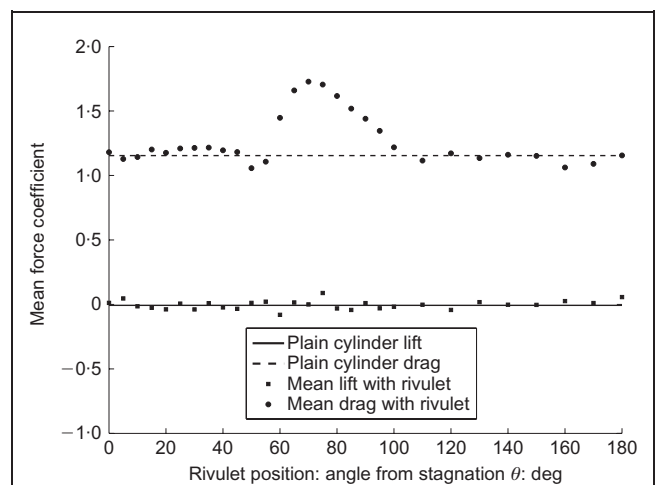


Figure 7. Variation of \bar{C}_D and \bar{C}_L with rivulet angle θ for the multiple symmetric artificial rivulet case

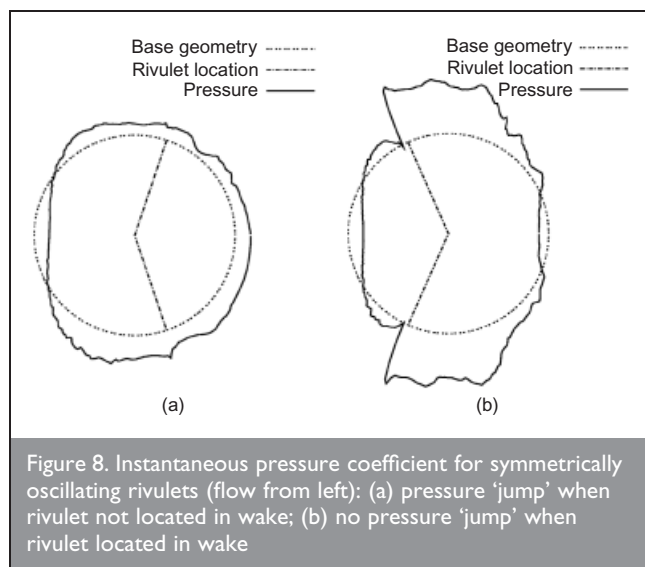
on the surface of the cylinder. Owing to the greater complexity of the flow field and larger number of variables, interpreting the results becomes increasingly difficult. Of particular interest are cases when the rivulet oscillates in the region where the changes in lift and drag were greatest in the static artificial rivulet analysis presented above. Furthermore, unless the rivulet is located within the wake, $\theta \geq 100^\circ$, markedly increased local 'jumps' in the pressure field can be seen as the flow is tripped by the rivulet before separation, as shown in Figure 8. The location of the flow reattachment on the cylinder surface and the subsequent effects that this has on the time-averaged aerodynamic forces depends on the frequency and amplitude of the oscillation. Full analysis of the oscillating rivulets case is ongoing and will be reported in the future.

4.2. Numerical analysis of the thin film of water

The evolution equation (Equation 11) is a fourth-order, non-linear, non-constant coefficient partial differential equation, and as such it cannot, in general, be solved analytically. Therefore, a pseudo-spectral (or collocation) method solver using an N point Fourier spectral mode in space and a fourth-order Adams–Bashforth time-marching algorithm was constructed. This numerical method was chosen specifically because of the periodic and continuous nature of the problem over the interval $\theta \in [0^\circ, 360^\circ)$, and the rapid rate of convergence it provides to the solution, given the presumed smoothness of the final result. Further details of the implementation of the pseudo-spectral method and parameter selection are given in Robertson *et al.* (2008).

Standard values for gravity and the properties at an air–water interface at 20°C were used throughout the present study and are listed in Table 2, while other parameter values were chosen to represent typical values for RWIV and to ensure the ratio of initial film thickness to cylinder radius $h_0/R = 6.3 \times 10^{-3}$ was consistent with those of previous experimental and computational studies by Flamand (1995) and Lemaitre *et al.* (2007). Accordingly, the Reynolds number implemented was a sub-critical value typical for RWIV of $Re = 10^5$.

The distributions of pressure and shear due to the external



aerodynamic field were assumed to be constant with time and therefore functions of θ only, that is $\mathbf{P} = \mathbf{P}(\theta)$ and $\mathbf{T} = \mathbf{T}(\theta)$, illustrated in Figure 9. These are based upon the mean pressure coefficient and normalised mean friction coefficients, \overline{C}_P and \overline{C}_F^* , for the external aerodynamic field around a dry cylinder, values for which were determined experimentally by Achenbach (1968) at a Reynolds number similar to that under investigation here of $Re = 10^5$. For the numerical investigation, 20-term Fourier series representations of \overline{C}_P and \overline{C}_F^* were used and appropriately scaled such that the maximum values of pressure and shear loadings matched those of Lemaitre *et al.* (2007), thus allowing direct comparisons between the results.

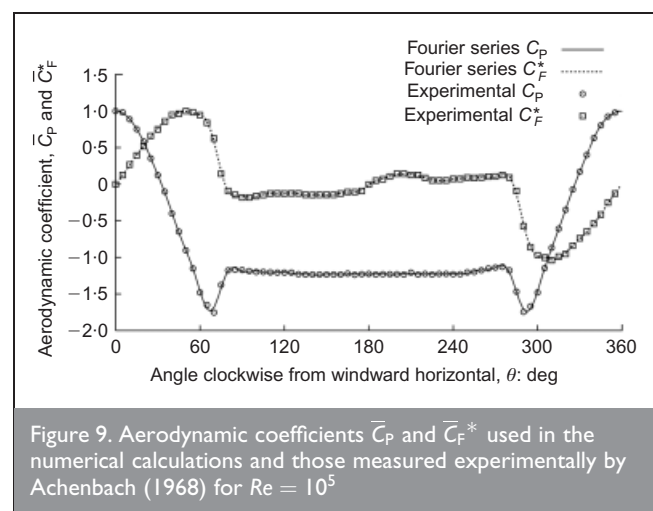
Three different combinations of the loadings, pressure \mathbf{P} , shear \mathbf{T} , surface tension $\boldsymbol{\gamma}$ and gravity \mathbf{g} were considered in this study. These were

- (a) shear and surface tension ($\mathbf{P} \equiv 0$ and $\mathbf{g} = 0$),
- (b) pressure and surface tension ($\mathbf{T} \equiv 0$ and $\mathbf{g} = 0$)
- (c) full loading (\mathbf{P} , \mathbf{T} , \mathbf{g} and $\boldsymbol{\gamma} \neq 0$).

4.2.1. Shear and surface tension loading. The temporal evolution of the thin film under the effect of shear \mathbf{T} and surface tension $\boldsymbol{\gamma}$ loading is shown in Figure 10. Under this combination, two distinct symmetrically placed rivulets form, one each on the upper and lower surfaces, with locations just windward of the clockwise and anticlockwise separation points for a dry cylinder at the same Re . As expected for this shear loading, the two rivulets are of equal height, profile and growth rate. This prediction is consistent with the previous experimental analysis of Bosdogianni and Olivari (1996), who

Parameter	Values
Cylinder radius, R	0.08 m
Initial film thickness, h_0	5×10^{-4} m
Gravity, g	9.806 m/s^2
Density of water, ρ	1000 kg/m^3
Dynamic viscosity of water, μ	$1.002 \times 10^{-3} \text{ Ns/m}$
Surface tension of water, $\boldsymbol{\gamma}$	$72 \times 10^{-3} \text{ N/m}$

Table 2. Values of the standard parameters used in the numerical calculations



indicate that the rivulets ‘form on the upper and lower surface of the cylinder at positions roughly corresponding to the expected separation points’. The results are also in good agreement with the only other computational results available for the same problem (Lemaitre *et al.*, 2007) illustrated in Figure 11, which demonstrates that the present results are virtually the same as those obtained by Lemaitre *et al.* (2007), at an evolution time of $t = 6.9 \times 10^{-3}$ s. Although both sets of results are numerical predictions, the governing evolution equations (Equation 11 from above, and Equation 17 from Lemaitre *et al.*, 2007) were independently derived and were solved by way of different procedures, thus verifying the computational results.

4.2.2. *Pressure and surface tension loading.* Under only pressure P and surface tension γ loading, the results show

distinct similarities to those for the previous case. Here again symmetric rivulets form just windward of the separation points on both sides of a dry cylinder (Figures 12 and 13). In this instance, however, the locations of these rivulets are marginally windward of those formed in the shear and surface tension case (Figure 13), with the ‘size’ of the rivulets under the present pressure loading being approximately the same order of magnitude as for the shear loading condition. When considered in conjunction with the similar rates of rivulet growth (Figures 10 and 12), the indication is that the effects of pressure and shear loadings are of a similar magnitude and therefore appear to be of broadly equal importance.

4.2.3. *Full loading.* The temporal evolution of film thickness for all four loading conditions (pressure, shear, surface tension and gravity) acting simultaneously is shown in Figure 14.

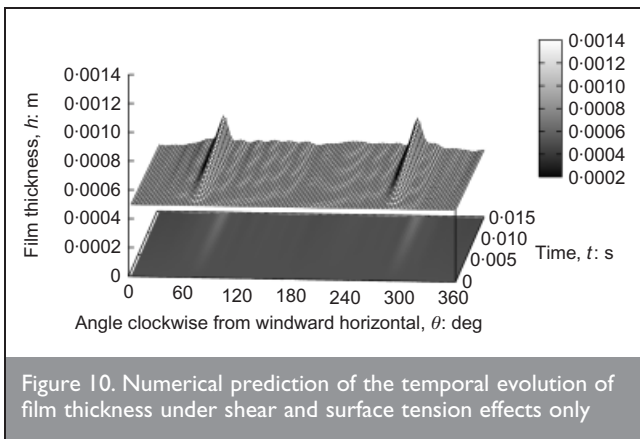


Figure 10. Numerical prediction of the temporal evolution of film thickness under shear and surface tension effects only

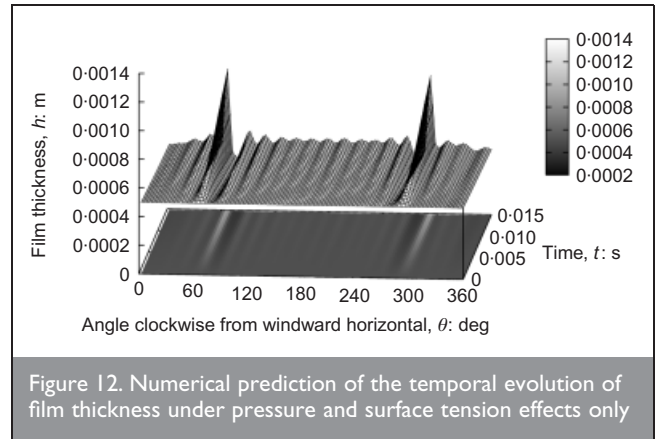


Figure 12. Numerical prediction of the temporal evolution of film thickness under pressure and surface tension effects only

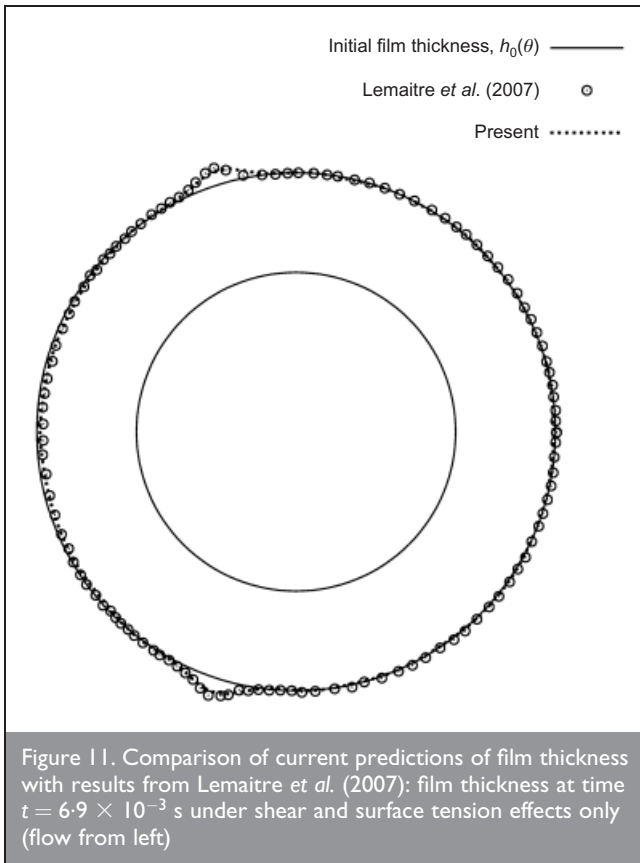


Figure 11. Comparison of current predictions of film thickness with results from Lemaitre *et al.* (2007): film thickness at time $t = 6.9 \times 10^{-3}$ s under shear and surface tension effects only (flow from left)

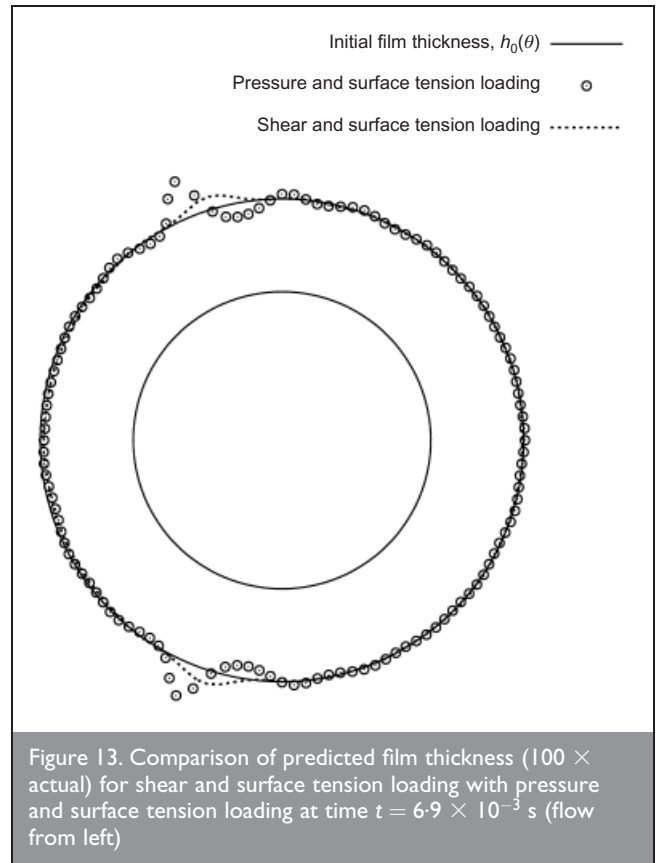


Figure 13. Comparison of predicted film thickness ($100 \times$ actual) for shear and surface tension loading with pressure and surface tension loading at time $t = 6.9 \times 10^{-3}$ s (flow from left)

Similarly to the previous two cases, under full loading conditions two distinct rivulets can be seen to form. However, in this instance the symmetry with respect to the incident flow between the upper and lower surfaces of the cylinder is lost due to the effect of gravity. The gravitational loading causes the rivulets to be thicker on the lower surface and thinner on the upper surface than those examined previously. The growth rate of the lower rivulet is also greater than that of the upper rivulet owing to the effect of gravitational loading, as would be expected. Furthermore, while the point of maximum thickness of the lower rivulet moves leeward from the point where it occurred under pressure and surface tension loading only, specifically from $\theta \approx 288^\circ$ to $\theta \approx 282^\circ$, the thinner upper rivulet moves windward from $\theta \approx 66^\circ$ to $\theta \approx 59^\circ$.

4.3. Fully coupled model

Research is ongoing to develop a fully coupled model using the rivulet evolution equation and the unsteady aerodynamic solver. The coupled model uses the pressure predicted by the unsteady solver as input to the rivulet evolution equation to determine the film thickness (gravity not included). The new surface distribution of the film is then used as input to the next time step of the aerodynamic solver, to determine the new external flow field and pressure, and the process is repeated. Images at various stages of the rivulet growth from initial simulations are illustrated in Figure 15. These preliminary results from this unique coupled model demonstrate the capability of this model to provide a numerical tool capable of simulating RWIV. The nature of the rivulets predicted by the unsteady coupled simulation are noticeably different from the results presented above that used a constant pressure distribution. This is as expected since in the above case, the pressure and shear distributions are unaffected by the formation of the rivulets, whereas in the coupled model the rivulet profile and shape, as well as the pressure and shear distributions, are changing in time. Most noticeably, two 'bulges' are formed on the upper and lower surfaces of the cylinder. The initial interpretation is that the upstream rivulet forms close to the separation point, and the downstream rivulet evolves owing to the reattachment of the shear layer. As the thickness of the upstream rivulet increases, the separation and reattachment of the shear layer is affected and the downstream rivulet moves forward. It does appear that for the wind speed used in this investigation, the rivulets move towards an 'equilibrium' angle (close to the separation point for a dry

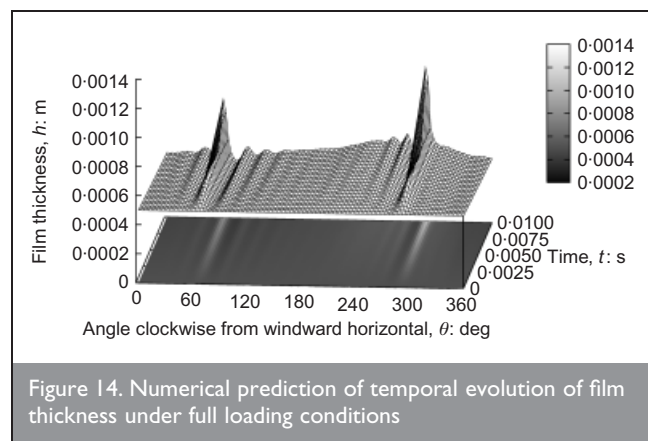


Figure 14. Numerical prediction of temporal evolution of film thickness under full loading conditions

cylinder), after which there is no apparent further motion, although the shapes of the rivulets are still changing with time. These results show that the method has the potential to allow a detailed investigation into the rivulet dynamics and their effect on the unsteady loading on the cylinder. However, the results and interpretations are preliminary and research is ongoing to develop the numerical model further.

5. CONCLUSIONS

RWIV is an active area of research, with the underlying physical mechanisms of the phenomenon still to be fully understood. At a recent international workshop on RWIV, the following key themes and areas for future research activity were identified.

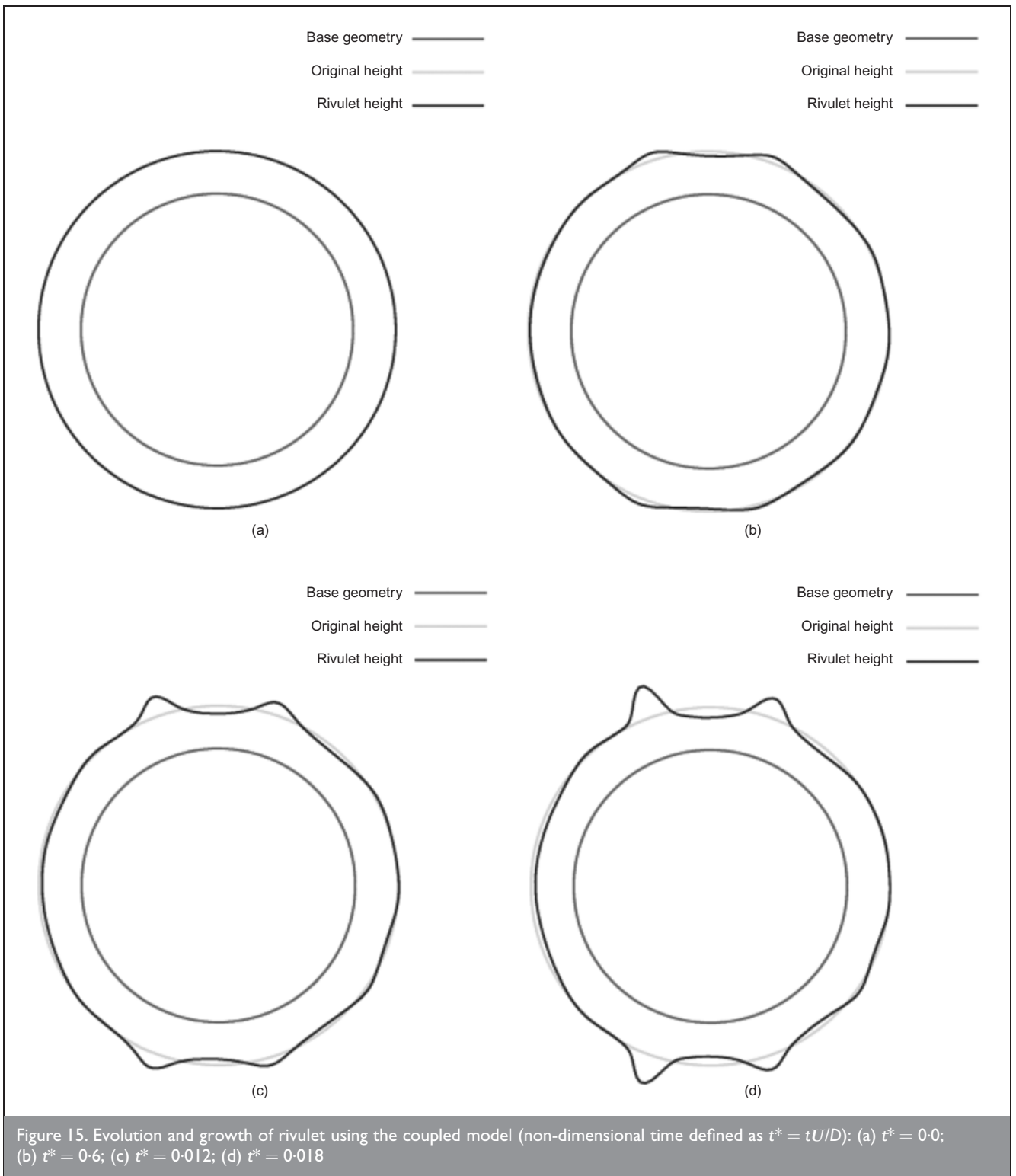
- RWIV is still not well understood.
- RWIV is related to, but distinct from, dry-inclined galloping.
- The presence of rivulets can act to increase the likelihood of a galloping-type oscillation.
- Vibrations often occur in flow regimes in which Karman vortex shedding is suppressed.
- RWIV often occurs in the critical Reynolds number range, though the full effect of the Reynolds number variation has not been fully established.
- The effect of the size, shape and location of the rivulet and the effect of surface characteristics has not been fully determined.
- Improved numerical methods are required to aid understanding of RWIV.

A numerical method to investigate aspects of RWIV has been developed at the University of Strathclyde, which uses an unsteady aerodynamic solver for the external aerodynamic field and a thin-film model based on lubrication theory to model the rivulet evolution and motion. Results from the new modelling approach are presented, and the main conclusions are as follows.

- Artificial rivulets on the cylinder modify the aerodynamic force coefficients (which vary with rivulet angle), and at particular rivulet configurations can cause a susceptibility to a galloping-type instability.
- Results obtained from the thin-film model are consistent with those in the literature. Under shear or pressure loading two symmetric rivulets form just windward of the separation points, while under full loading conditions the rivulets are asymmetric owing to the additional effect of gravity.
- Preliminary results from a fully coupled model demonstrate how the changing flow field influences the rivulet motion and growth.

ACKNOWLEDGEMENTS

The authors would like to thank the University of Strathclyde Research Enhancement Fund for providing the funds for the international workshop. We would also like to thank all the delegates who attended the workshop for entering into a full and open discussion. Without the willingness of these delegates kindly to offer their time and expertise, the workshop would not have been a success: Dr Xiaoping Du, Dr Olivier Flamand,



Dr Pascal Hemon, Dr John Macdonald, Professor Masaru Matsumoto, Dr Tomomi Yagi and Dr Delong Zuo.

Thanks also to Mrs Irene Spencer, Department of Mathematics, University of Strathclyde, for undertaking many of the organisational arrangements for the workshop.

The authors A. C. Robertson and J. M. Sullivan gratefully acknowledge the support of the UK Engineering and Physical Sciences Research Council (EPSRC) through Doctoral Training Account studentships.

APPENDIX

Derivation of thin film equations

Two-dimensional, unsteady flow of a thin film of incompressible viscous fluid with uniform dynamic viscosity μ and density ρ on the outer surface of a stationary horizontal circular cylinder of radius R is considered. The free surface of this film is subject to a prescribed normal stress ('pressure'), $\mathbf{P} = \mathbf{P}(\theta, t)$, and prescribed tangential stress ('shear'), $\mathbf{T} = \mathbf{T}(\theta, t)$, exerted by the external aerodynamic field (Figure 4), as a function of clockwise angle from the

windward (left-hand) horizontal, θ ($0^\circ \leq \theta \leq 360^\circ$), and time, t .

Model description

The film is taken to be thin, its aspect ratio ε (defined by $\varepsilon = H/R$, where H denotes a typical film thickness) satisfying $\varepsilon \ll 1$ (Figure 4). Initially the description is referred to polar coordinates r, θ, z with the z axis along the axis of the cylinder and with θ ($-\pi < \theta \leq \pi$) measured from the horizontal on the upstream (left-hand) side of the cylinder; then the surface of the cylinder is given by $r = R$. The film thickness is denoted by $h = h(\theta, t)$ (unknown *a priori*); then the free surface of the film is given by $r = R + h$. Near any station $\theta = \text{constant}$ the description may alternatively be referred to a local Cartesian coordinate system $Oxyz$ with Ox tangential to the cylinder (increasing in the direction of increasing θ , so that $x = R\theta + \text{constant}$) and Oy along the outward normal to the cylinder, with y defined by $y = r - R$, so that the cylinder is at $y = 0$ and the free surface is at $y = h$. In the latter coordinate system the governing mass-conservation and Navier–Stokes equations give, at leading order in ε

$$12 \quad u_x + v_y = 0$$

$$13 \quad 0 = -p_x - \rho g \cos \theta + \mu u_{yy}$$

$$14 \quad 0 = -p_y$$

where

$$u(r, \theta) = iu(r, \theta) + jv(r, \theta)$$

and

$$15 \quad g = -g(i \cos \theta + j \sin \theta)$$

Equations 12 to 14 are subject to the no-slip and no-penetration conditions on the cylinder

$$16 \quad u = v = 0 \text{ on } y = 0$$

and at the free surface, to the kinematic condition

$$17 \quad v = h_t + uh_x \text{ on } y = h$$

the tangential stress condition

$$18 \quad \mu u_y = T \text{ on } y = h$$

and the normal stress condition

$$19 \quad p = \gamma \kappa + P \text{ on } y = h$$

where γ is the coefficient of surface tension, and κ is the mean curvature of the free surface, given to first order by

$$20 \quad \kappa = \frac{1}{R} - \frac{1}{R^2}(h + h_{\theta\theta})$$

The azimuthal volume flux of fluid in the film is given by

$$21 \quad Q = \int_0^h u \, dy$$

and using this and Equation 12, it is possible to replace Equation 17 by the conservation law

$$22 \quad h_t + Q_x = 0$$

Evolution equation for $h(\theta, t)$

Integrating Equation 14 subject to Equation 19 yields

$$23 \quad p = \gamma \kappa + P$$

(independent of y), and then integrating Equation 13 with respect to y subject to Equation 16 and 18 gives

$$24 \quad u = -\frac{1}{2\mu}(\rho g \cos \theta + p_x)(2hy - y^2) + \frac{Ty}{\mu}$$

Therefore from Equation 21

$$25 \quad Q = -\frac{1}{3\mu}(\rho g \cos \theta + p_x)h^3 + \frac{Th^2}{2\mu}$$

Finally, substituting Equation 25 into Equation 22 and using Equations 20 and 23 leads to the evolution equation for $h(\theta, t)$

$$26 \quad h_t + \left\{ -\frac{1}{3\mu R} \left[\rho g \cos \theta - \frac{\gamma}{R^3}(h + h_{\theta\theta})_\theta + \frac{P_\theta}{R} \right] \times h^3 + \frac{Th^2}{2\mu R} \right\}_\theta = 0$$

REFERENCES

- Achenbach E (1968) Distribution of local pressure and skin friction around a circular cylinder in a cross flow up to $Re = 5 \times 10^6$. *Journal of Fluid Mechanics* **34**(4): 625–639.
- Bosdogianni A and Olivari D (1996) Wind- and rain-induced oscillations of cables of stayed bridges. *Journal of Wind Engineering and Industrial Aerodynamics* **64**(2-3): 171–185.
- Cosentino N, Flamand O and Ceccoli C (2003) Rain-wind induced vibration of inclined stay cables. Part 1: experimental investigation and physical explanation. *Wind and Structures* **6**(6): 471–484.
- Flamand O (1995) Rain-wind induced vibration of cables.

- Journal of Wind Engineering and Industrial Aerodynamics* 57(2–3): 353–362.
- Geurts C, Vrouwenfelder T, Van Staalduinen P and Reusink J (1998) Numerical modelling of rain-wind-induced vibration: Erasmus Bridge, Rotterdam. *Structural Engineering International, Journal of the International Association for Bridge and Structural Engineering* 8(2): 129–135.
- Gu M, Liu CJ, Xu YL and Xiang HF (2002) Response characteristics of wind excited cables with artificial rivulet. *Applied Mathematics and Mechanics* 23(10): 1176–1187.
- Gu M and Du X (2005) Experimental investigation of rain-wind-induced vibration of cables in cable-stayed bridges and its mitigation. *Journal of Wind Engineering and Industrial Aerodynamics* 93(1): 79–95.
- Gu M (2007) Study on wind-rain induced vibration of stay cables of cable-stayed bridges based on quasi-steady assumption. *Proceedings of the 12th International Conference on Wind Engineering, Cairns*, 1: 18–40.
- Gu M and Huang L (2008) Theoretical and experimental studies on the aerodynamic instability of a two-dimensional circular cylinder with a moving attachment. *Journal of Fluids and Structures* 24(2): 200–211.
- Hikami Y and Shiraishi N (1988) Rain-wind induced vibrations of cables in cable stayed bridges. *Journal of Wind Engineering and Industrial Aerodynamics* 29(1–3): 409–418.
- Holland D, Duffy BR and Wilson SK (2001) Thermocapillary effects on a thin viscous rivulet draining steadily down a uniformly heated or cooled slowly varying substrate. *Journal of Fluid Mechanics* 441: 195–221.
- Lemaitre C, Hemon P and De Langre E (2007) Thin water film around a cable subject to wind. *Journal of Wind Engineering and Industrial Aerodynamics* 95(9–11): 1259–1271.
- Li SY and Gu M (2006) Numerical simulations of flow around stay cables with and without fixed artificial rivulets. *Proceedings of the 4th International Symposium on Computational Wind Engineering (CWE2006), Yokohama*, 307–310.
- Liu Q, Matsumoto M, Yagi T and Hori K (2007) LES study on the mechanism of rain-wind induced vibration of cables of cable-stayed bridge. *Proceedings of the 12th International Conference on Wind Engineering, Cairns*, 1: 895–902.
- Macdonald JHG and Larose GL (2008a) Two-degree-of-freedom inclined cable galloping. Part 1: general formulation and solution for perfectly tuned system. *Journal of Wind Engineering and Industrial Aerodynamics* 96(3): 291–307.
- Macdonald JHG and Larose GL (2008b) Two-degree-of-freedom inclined cable galloping. Part 2: analysis and prevention for arbitrary frequency ratio. *Journal of Wind Engineering and Industrial Aerodynamics* 96(3): 308–326.
- Matsumoto M, Saitoh T, Kitazawa M, Shirato H and Nishizaki T (1995) Response characteristics of rain-wind induced vibration of stay-cables of cable-stayed bridges. *Journal of Wind Engineering and Industrial Aerodynamics* 57(2–3): 323–333.
- Matsumoto M, Yagi T, Shigemura Y and Tsushima D (2001) Vortex-induced cable vibration of cable-stayed bridges at high reduced velocity. *Journal of Wind Engineering and Industrial Aerodynamics* 89(7–8): 633–647.
- Matsumoto M, Yagi T, Goto M and Sakai S (2003) Rain-wind induced vibration of inclined cables at limited high reduced wind velocity region. *Journal of Wind Engineering and Industrial Aerodynamics* 91(1): 1–12.
- Matsumoto M, Yagi T, Hatsuda H, Shima T and Tanaka M (2007a) Sensitivity of dry-state galloping of cable stayed bridges to Scruton number. *Proceedings of 7th International Conference on Cable Dynamics, Vienna*, paper no. 6.
- Matsumoto M, Yagi T, Adachi Y, Hatsuda H and Shima T (2007b) Karman vortex effects on aerodynamic instabilities of inclined stay-cables. *Proceedings of the 12th International Conference on Wind Engineering, Cairns*, 1: 175–182.
- Matsumoto M, Hashimoto M, Yagi T, Nakase T and Maeta K (2008) Study on the role of Karman Vortex on galloping of bluff bodies. *Proceedings of the 9th International Conference on Flow-Induced Vibration – FIV2008, Prague*, 687–692.
- Ni YQ, Wang XY, Chen ZQ and Ko JM (2007) Field observations of rain-wind-induced cable vibration in cable-stayed Dongting Lake Bridge. *Journal of Wind Engineering and Industrial Aerodynamics* 95(5): 303–328.
- Peil U and Dreyer O (2007) Rain-wind induced vibrations of cables in laminar and turbulent flow. *Wind and Structures* 10(1): 83–97.
- Robertson AC and Taylor IJ (2007) Effect of rivulets on a circular cylinder using a 2D discrete vortex method. *Proceedings of the 12th International Conference on Wind Engineering, Cairns*, 1: 863–870.
- Robertson AC, Taylor IJ, Wilson SK, Duffy BR and Sullivan JM (2008) A model for the numerical simulation of rivulet evolution on a circular cylinder in an air flow. *Proceedings of the 9th International Conference on Flow-Induced Vibration – FIV2008, Prague*, 693–698.
- Seidel C and Dinkler D (2006) Rain-wind induced vibrations – phenomenology, mechanical modelling and numerical analysis. *Computers and Structures* 84(24–25): 1584–1595.
- Sullivan JM, Wilson SK and Duffy BR (2008) A thin rivulet of perfectly wetting fluid subject to a longitudinal surface shear stress. *Quarterly Journal of Mechanics and Applied Mathematics* 61(1): 25–61.
- Sullivan JM (2009) *Thin-film flows subject to an external shear stress*. PhD Thesis, Department of Mathematics, University of Strathclyde, Glasgow.
- Taylor IJ and Vezza M (1999) Prediction of unsteady flow around square and rectangular section cylinders using a discrete vortex method. *Journal of Wind Engineering and Industrial Aerodynamics* 82(1–3): 247–269.
- Taylor IJ and Vezza M (2001) Application of a discrete vortex method for the analysis of suspension bridge deck section. *Wind and Structures* 4(4): 333–352.
- Taylor IJ and Vezza M (2002) Aeroelastic stability analysis of a bridge deck with added vanes using a discrete vortex method. *Wind and Structures* 5(2–4): 277–290.
- Verwiebe C and Ruscheweyh H (1998) Recent research results concerning the exciting mechanisms of rain-wind-induced vibrations. *Journal of Wind Engineering and Industrial Aerodynamics* 74–76, 1005–1013.
- Wang ZJ, Zhou Y, Huang JF and Xu YL (2005) Fluid dynamics around an inclined cylinder with running water rivulets. *Journal of Fluids and Structures* 21(1), 49–64.
- Wilson SK and Duffy BR (2005) Unidirectional flow of a thin rivulet on a vertical substrate subject to a prescribed uniform shear stress at its free surface. *Physic of Fluids* 17(10): 108–105.
- Yamaguchi H (1990) Analytical study on the growth mechanism of rain vibration of cables. *Journal of Wind Engineering and Industrial Aerodynamics* 33(1–2), 78–80.

Yeo D and Jones NP (2008) Investigation on 3-D characteristics of flow around a yawed and inclined circular cylinder. *Journal of Wind Engineering and Industrial Aerodynamics* 96(10–11): 1947–1960.

Zuo D, Jones NP and Main JA (2008) Field observation of vortex- and rain-wind-induced stay-cable vibrations in a three-dimensional environment. *Journal of Wind Engineering and Industrial Aerodynamics* 96(6–7): 1124–1133.

What do you think?

To discuss this paper, please email up to 500 words to the editor at journals@ice.org.uk. Your contribution will be forwarded to the author(s) for a reply and, if considered appropriate by the editorial panel, will be published as discussion in a future issue of the journal.

Proceedings journals rely entirely on contributions sent in by civil engineering professionals, academics and students. Papers should be 2000–5000 words long (briefing papers should be 1000–2000 words long), with adequate illustrations and references. You can submit your paper online via www.icevirtuallibrary.com/content/journals, where you will also find detailed author guidelines.